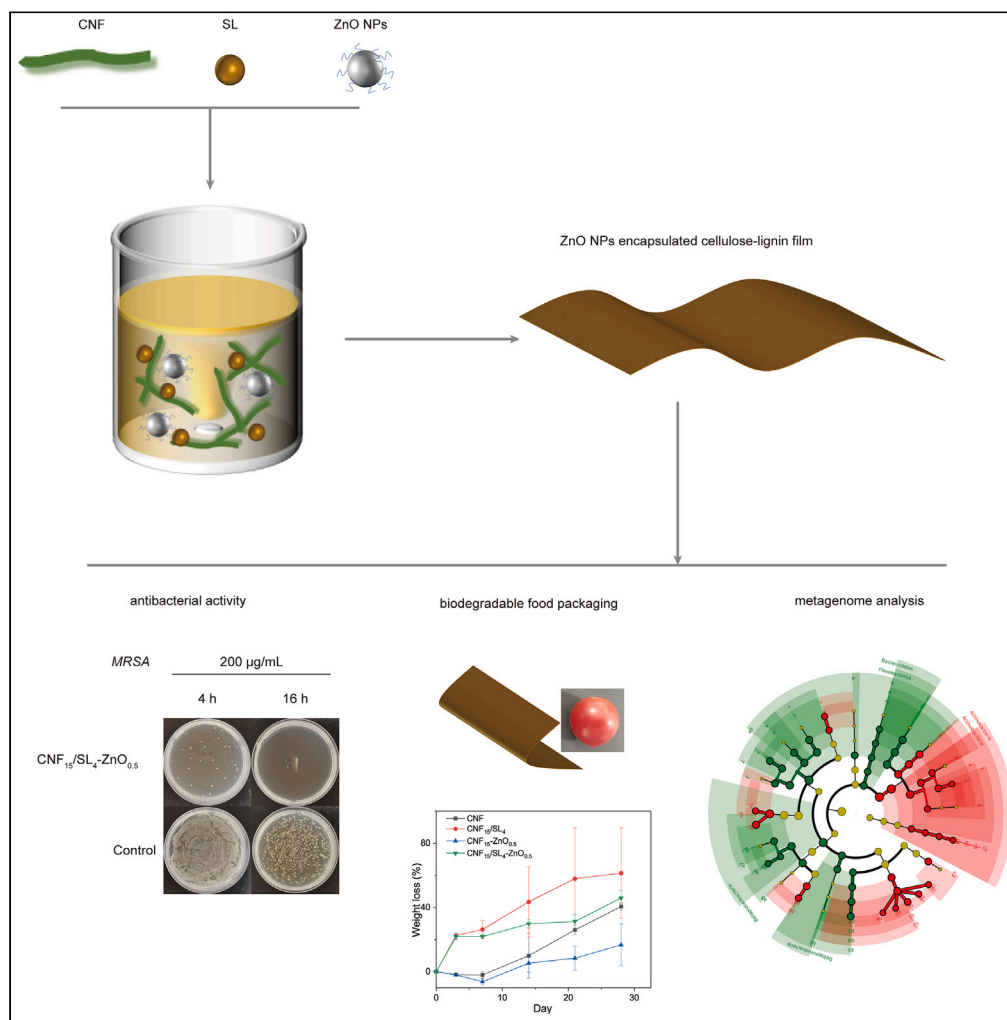


Article

ZnO nanoparticles encapsulated cellulose-lignin film for antibacterial and biodegradable food packaging



Xinyi Zhu, Henghui Li, Ling Cai, ..., Hao Wang, Daorong Wang, Jin Chen

jchen@njmu.edu.cn

Highlights

Nano-ZnO loaded sodium lignosulfonate (SL)-cellulose nanofibers (CNFs) film is made

CNF/SL-ZnO composite films exhibit UV-blocking, antioxidant, and biocidal effect

CNF/SL-ZnO films exhibit desirable thermal stability and biodegradability

CNF/SL-ZnO films as food packaging shows an improved shelf life



Article

ZnO nanoparticles encapsulated cellulose-lignin film for antibacterial and biodegradable food packaging

Xinyi Zhu,^{1,2,3,8} Henghui Li,^{1,2,8} Ling Cai,^{1,2,4} Yixian Wu,⁵ Jun Wang,^{1,2} Shangcheng Xu,¹ Shoulin Wang,² Hao Wang,⁶ Daorong Wang,⁶ and Jin Chen^{1,2,4,7,9,*}

SUMMARY

Foodborne illness caused by consuming foods contaminated by pathogens remains threatening to the public health. Despite considerable efforts of using renewable source materials, it is highly demanding to fabricate food packaging with multiple properties including eco-friendliness, bactericidal effect and biocompatibility. Here, sodium lignosulfonate (SL) and ZnO nanoparticles (ZnO NPs) were used as functional filler and structure components, respectively, on the cellulose nanofibers (CNFs)-based films, which endows the produced membrane (CNF/SL-ZnO) the UV-light blocking, antioxidant, and antimicrobial characteristics. Due to the interconnected polymeric structure, the prepared CNF/SL-ZnO films possessed considerable mechanical properties, thermal stability, and good moisture barrier capability. Moreover, the tested samples exhibited an improved shelf life in food packaging. Furthermore, metagenome analysis revealed superior biodegradability of obtained films with negligible side effect on the soil microenvironment. Therefore, the biocompatible, degradable, and antibacterial CNF/SL-ZnO film holds enormous potential for sustainable uses including food packaging.

INTRODUCTION

The spread of foodborne pathogen especially during logistics process as typified by the recent COVID-19 pandemic has urged the search for food packaging materials with multiple properties including long shelf life, high sustainability and superior antimicrobial effect.^{1–4} However, because of outstanding mechanical and barrier properties and low cost, the current commercial food packaging is mainly derived from petroleum-based polymers such as polyvinylchloride (PVC) and polyethylene terephthalate (PET), in which more than 30% of worldwide production of plastics is used for food packaging.⁵ Consequently, the increasing consuming and disposal of these plastic materials that are resistant to degradation has caused considerable environmental concerns for the public health. It is estimated that ~300 million tons of plastics are annually produced around the world, but only a small portion of ~2% can be recycled and reused.^{6,7} Moreover, their extremely low degradability makes them accumulate in landfills or natural environment rather than decompose,^{8,9} which demands the development of sustainable and renewable resources in the last decades as the global population increases.^{10,11}

Lignocellulose biomass consisted of cellulose, hemicellulose, and lignin, is widely found in the naturally plants, such as trees, flax, cottons, and sugarcanes.¹² Being the structural component of primary cell wall, cellulose constitutes the most abundant biopolymer in the earth.^{13,14} In particular, cellulose nanofibers (CNFs) with an average diameter of approximately 5–60 nm and several micrometers in length, are promising cellulose derivatives as natural, inexpensive, and eco-friendly nanomaterials with unique physical properties.^{9,15} Taken these advantageous attributes, considerable efforts of using CNFs as candidate materials for plastic replacement have been witnessed recently.¹⁶ Nevertheless, the presence of abundant hydroxyl groups in its structure brings the water instability to the cellulose material, which requires additional structural modifications to increase its performance.¹⁷

As the structural support to hold cellulose fibers together in the plant like wood, lignin is the second-most abundant biopolymer in the world,¹³ which is mainly consisted of 3 constituent monomers (guaiacyl alcohol, syringyl alcohol, and p-hydroxyl alcohol) via oxidative

¹The Affiliated Chongqing Prevention and Treatment Center for Occupational Diseases, School of Public Health, Nanjing Medical University, Chongqing 400060, China

²The Key Laboratory of Modern Toxicology, Ministry of Education, Center for Global Health, School of Public Health, Nanjing Medical University, Nanjing 211166, China

³Taizhou Center for Disease Control and Prevention, Taizhou 318000, China

⁴School of Chemistry and Chemical Engineering, Southeast University, Nanjing 211189, China

⁵Department of Health Promotion Center, The First Affiliated Hospital of Nanjing Medical University, Nanjing 210029, China

⁶Northern Jiangsu People's Hospital Affiliated to Nanjing Medical University, Yangzhou 225001, China

⁷Jiangsu Province Engineering Research Center of Antibody Drug, Key Laboratory of Antibody Technique of National Health Commission, Nanjing Medical University, Nanjing 211166, China

⁸These authors contributed equally

⁹Lead contact

*Correspondence: jchen@njmu.edu.cn

<https://doi.org/10.1016/j.isci.2024.110008>



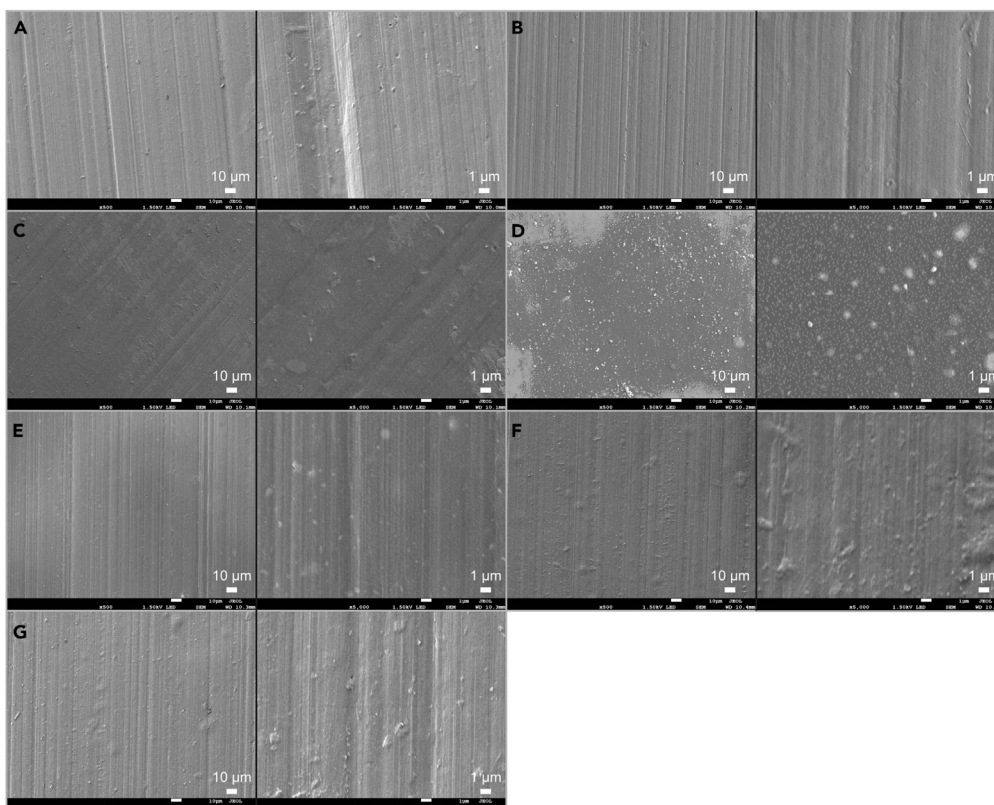


Figure 1. Representative SEM images of films

(A–G) Pure CNF film (A) and composite films: CNF₁₅/SL₂ (B), CNF₁₅/SL₄ (C), CNF₁₅/SL₈ (D), CNF₁₅/SL₂-ZnO_{0.5} (E), CNF₁₅/SL₄-ZnO_{0.5} (F), and CNF₁₅-ZnO_{0.5} (G). The scale bars in each sample were 10 μm (left) and 1 μm (right), respectively.

coupling.^{18,19} Due to the richness of functional groups including ketones, phenolic units, and phenolic hydroxyl groups, lignin possesses advantageous features in UV shielding, antioxidant and water-proof applications.^{20,21} However, the annual production of lignin is ~50 million tons with a small portion (1–2%) is utilized pointing to its role of underutilized material.^{1,22} Inspired by the structural composition of the wood, lignin in combination of cellulose materials can be explored for value-added products.²³



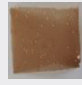



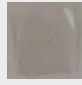
In this study, CNFs, sodium lignosulfonate (SL), and ZnO nanoparticles (ZnO NPs) were blended using a solution casting method to obtain the composite film for food packaging. Currently, foodborne pathogens, such as *Staphylococcus aureus* and *Listeria monocytogenes*, are mainly responsible for food illness and even deaths. To overcome the poor antimicrobial activity of cellulose and lignin,²⁴ nanomaterials of biocidal effect have been attempted in the packaging materials to improve their mechanical properties while maintaining the biodegradable and eco-friendly characteristic.²⁵ As a generally recognized as safe (GRAS) substance by the US Food and Drug Administration (FDA), ZnO NPs have been extensively explored as a reinforcing and functional filler with refined mechanical as well as antibacterial properties.^{26–28} Lignosulfonates are typical by-products from the sulfite pulping process in paper industry and have desirable water solubility for practical uses. Therefore, by combing CNFs, SL, and ZnO NPs at optimized weight ratio, high-performance composite films were obtained and their mechanical properties, antibacterial, and antioxidant abilities were studied. Moreover, the biocompatibility and food preservation ability of the films were evaluated. Furthermore, soil burial test was conducted to examine the biodegradability and metagenome analysis was performed to provide insights of the composition and function of soil microbiota.

RESULTS

Characterization of synthesized films

SEM was used to evaluate the surface morphological features of the obtained composite films. SEM images of seven films at 500× and 5,000× magnifications were shown in Figure 1. Pure CNF film exhibited homogeneous, smooth, and compact surfaces (Figure 1A). A relatively small amount of SL addition causes no apparent changes in the density in CNF₁₅/SL₂ and CNF₁₅/SL₄ films (Figures 1B and 1C). However, as shown Figure 1D, excessive addition of SL caused the obvious aggregates resulting in the increase of roughness, indicating the presence of micro-phase separation. It was observed that the blending of ZnO NPs in pure CNF or CNF/SL composite films led to a slight heterogeneous, but no significant disruption of structural compactness when the mass ratio of CNFs and ZnO NPs was fixed as 15:0.5 (Figures 1E–1G). Compared with that of CNF₁₅/SL₂-ZnO_{0.5}, double dose of ZnO NPs in CNF₁₅/SL₂-ZnO₁ film made obvious unevenness and agglomerates visualized

Table 1. Physical and mechanical properties of different composite films

Sample	Appearance	Thickness (μm)*	Tensile strength (MPa)*	Elongation at break (%)*
CNF		28.5 ± 3.8^a	43.40 ± 10.83^a	14.71 ± 7.22^{ab}
CNF ₁₅ /SL ₂		31.0 ± 4.0^{ab}	40.76 ± 5.45^a	22.27 ± 7.82^{acd}
CNF ₁₅ /SL ₄		31.4 ± 3.0^{ab}	36.01 ± 3.15^{ab}	28.87 ± 5.49^{ad}
CNF ₁₅ /SL ₈		35.1 ± 4.6^c	22.54 ± 6.97^{bc}	37.16 ± 7.71^d
CNF ₁₅ /SL ₂ -ZnO _{0.5}		33.4 ± 3.6^b	20.87 ± 1.25^{bd}	5.60 ± 0.58^b
CNF ₁₅ /SL ₄ -ZnO _{0.5}		35.2 ± 4.0^c	70.06 ± 3.52	8.74 ± 2.77^{bc}
CNF ₁₅ -ZnO _{0.5}		37.1 ± 1.9^c	29.66 ± 5.26^{abcd}	7.91 ± 3.51^{bc}

*Same lowercase letters in the same column indicates no significant differences. Data are represented as mean \pm SD.

(Figure S1). Therefore, SL and ZnO NPs of appropriate amount of addition had good compatibility and dispersion with CNF matrix, which suggested a possible interaction among the components.

Thickness of different composite films was listed in Table 1. The thickness of CNF was measured to be $28.5 \mu\text{m}$, which was the lowest among all the samples. CNF₁₅/SL₂ and CNF₁₅/SL₄ showed no significant change of thickness, while a significant increase in thickness was observed for CNF₁₅-ZnO_{0.5} as compared to CNF, indicating that SL and ZnO NPs could be well integrated into the matrix, but ZnO NPs may cause slight changes in the film structure, which was consistent with the observation of SEM. The increase of thickness of CNF₁₅/SL₈ was due to the increase of total mass of materials for the preparation of the uniform film.¹⁶

To tolerate the stress during the handing, storage and shipping, food packaging materials often requires high mechanical properties. It should be noted that tensile strength (TS) and elongation at break (EB) are associated with the fabricated films' intermolecular forces and network microstructure. As shown in Table 1, TS and EB of samples were measured. As the addition of SL was increased, the TS exhibited a downtrend while EB showed the opposite, which was related to the combinational use of CNFs and SL in the film. When SL was added as well as the phenolic content increased, the intermolecular or intramolecular interactions formed between molecular chains of CNFs were weakened, resulting in the improved extensibility properties of the films. Particle polymerization, phase separation, and elastic collision between nanoparticles occurred with ZnO NPs added into CNFs, and the mobility of the macromolecules was decreased to some extent in the presence of ZnO NPs in the film environment, resulting in the relatively low TS and EB of CNF₁₅-ZnO_{0.5}.²⁹ By comparison, significant increase of TS in CNF₁₅/SL₄-ZnO_{0.5} was observed attributing to the interfacial adhesion from the multiple hydrogen bonds formed at an appropriate molar ratio of different components. In essence, the large specific surface area and high surface energy of ZnO NPs may promote the interfacial bonding and improve the strength of the film. Nevertheless, the mobility of the CNF₁₅/SL₄-ZnO_{0.5} film was limited due to the formation of its stable network structure, as visualized in the SEM images. Therefore, CNF₁₅/SL₄-ZnO_{0.5} with improved TS and retained flexibility was chosen for following studies, in which CNFs, CNF₁₅/SL₄, and CNF₁₅-ZnO_{0.5} were used as control.

As shown in Figures 2A and 2B, the thermo gravimetric analysis (TGA) and derivative thermo gravimetry (DTG) spectra of samples were recorded to examine the thermal stability of film. As reported, the sample mass loss ranging from 30 to 180°C was related to the water evaporation.³⁰ It was observed that the most significant weight loss of samples ranging from 220 to 340°C corresponding to the peak in their DTG spectra was attributed to the degradation of PEG modified on the surface of ZnO NPs in the matrix of CNFs and SL.¹⁸ The maximum

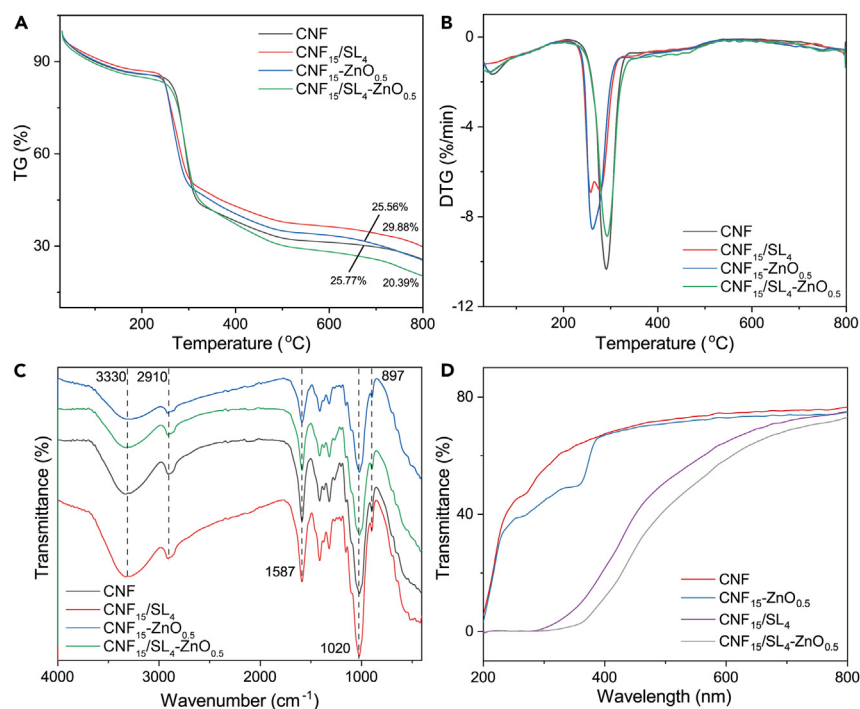


Figure 2. Characterization of composite films

(A–D) TGA (A), DTG (B), FTIR-ATR (C) and UV-vis diffuse reflectance (D) spectra of different composite films.

degradation temperature of CNF, CNF₁₅/SL₄, CNF₁₅/SL₄-ZnO_{0.5}, and CNF₁₅-ZnO_{0.5} was 290.5°C, 277.1°C, 292.5°C, and 261.7°C, respectively. The respective addition of SL and ZnO NPs into CNFs slightly decreased the thermal ability of the composite, but the thermal ability of CNF₁₅/SL₄-ZnO_{0.5} was improved due to the formation of relatively strong interfacial bonding.

Fourier transform infrared spectroscopy-attenuated total reflection (FTIR-ATR) spectra of samples were measured to study the functional groups as well as molecular interactions between the components of the films (Figure 2C). All the tested films exhibited typical broad absorption at 3,330 cm⁻¹ which was attributed to O–H stretching coupled with hydrogen.³¹ And peaks at 2,910 and 1,020 cm⁻¹ were associated with C–H and C–C stretching vibration, respectively. The peak found at 1,587 cm⁻¹ was related to the asymmetric stretching vibration of the carboxyl group, while peaks in the range of 1,500–1,300 cm⁻¹ were due to C–O elongation. Additionally, the small band at 897 cm⁻¹ was attributed to the C–O–C stretching vibrations band.³² As compared to the FTIR-ATR spectrum of CNFs, other samples displayed no new peak formation with some shifted peaks, indicating that the chemical structure of CNFs were not changed and the matrix was compatible with SL and ZnO NPs.³³

Optical properties such as ultraviolet barriers and transparency are important characteristics of food packaging films. The exposition to light especially ultraviolet can cause spoilage or fast quality loss of packaged food due to the lipid oxidation, color and moisture loss, and thereby bad taste effect. UV-blocking ability and high transparency are important characteristics of food protection and it will enable consumers to get a clear view of packaged food. The UV-vis diffuse reflectance spectra of films were shown in Figure 2D. CNF film showed high transmittance in UV-B (280–320 nm), UV-A (320–400 nm), and visible light (>400 nm) while the addition of ZnO NPs reduced the transmittance of UV light. The UV-barrier property of CNF₁₅/SL₄ and CNF₁₅/SL₄-ZnO_{0.5} was significantly enhanced owing to the richness of UV-absorbing functional groups of SL. Notably, all the films exhibited high transparency (transmittance at 660 nm > 65%).³⁴

Antibacterial and antioxidant activity

Figure 3 showed the recorded images of agar plates of Gram-negative *E. coli* and Gram-positive *S. aureus* and methicillin-resistant *Staphylococcus aureus* (MRSA). It was evident that a large number of colonies were formed on the control's agar plates when the incubation time was set as 4 and 16 h, respectively, indicating there is no observable bacterial cells death occurred. For CNF and CNF₁₅/SL₄, no antibacterial effect was observed as the density of colonies was similar with that of the control group. When treated with CNF₁₅-ZnO_{0.5}, there were decreased colonies visualized on the plate even at relatively long incubation time up to 16 h, pointing to a long-term antimicrobial activity mainly due to the presence of ZnO NPs in the film. Notably, CNF₁₅/SL₄-ZnO_{0.5} showed improved bactericidal effect against three model bacteria compared with that of CNF₁₅-ZnO_{0.5}, which indicated an enhancement of antibacterial effect of SL on ZnO NPs.

Agar diffusion assay and SEM observation were further conducted to evaluate the bacteria growth on the surface of the films. As shown in Figure S2A, colonies were distributed uniformly on the agar plate in the control group. When treated with CNF and CNF₁₅/SL₄ samples, the

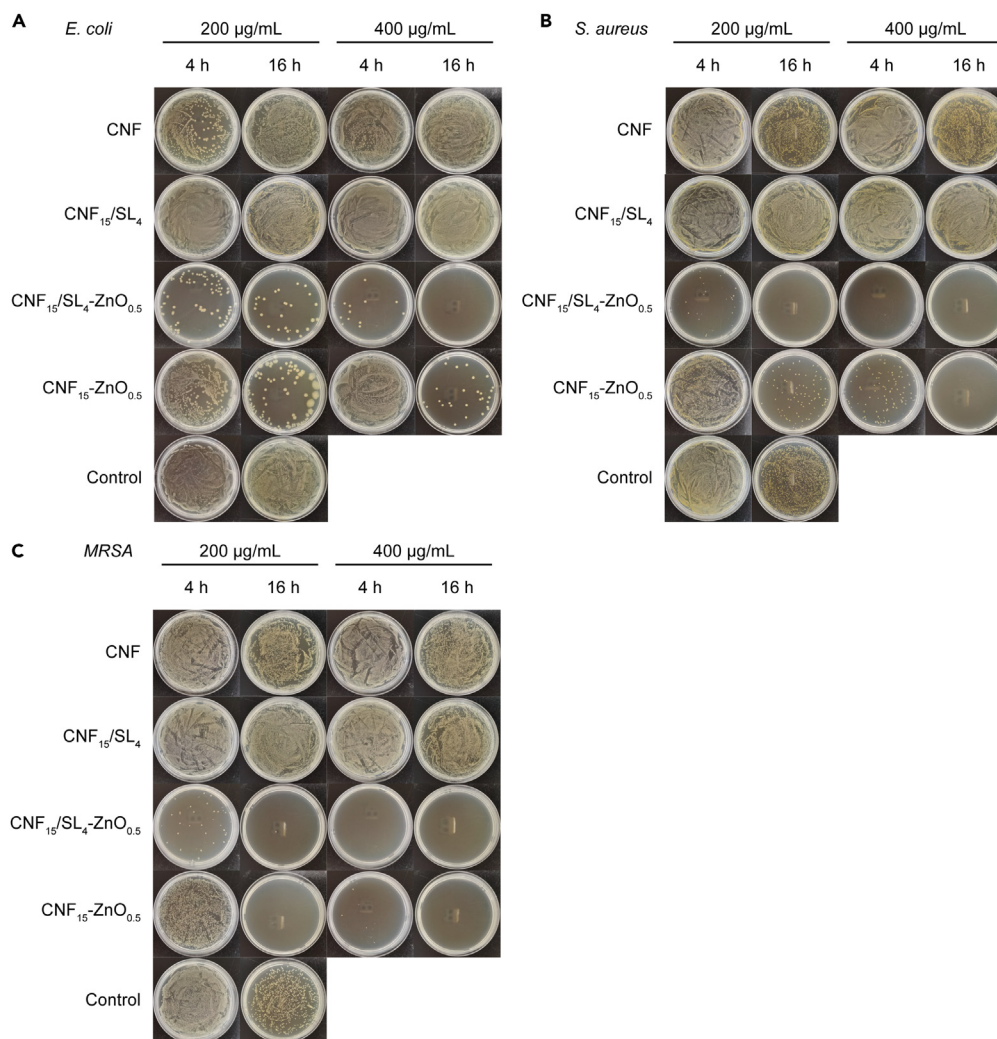


Figure 3. Antibacterial activity of different composite films

(A–C) The antibacterial activities were exhibited as the images of agar plates under treatments of films at series concentrations against *E. coli* (A), *S. aureus* (B), and MRSA (C) of 10^6 CFU/mL after different incubation time.

bacteria growth was not significantly affected. By contrast, after treated with CNF₁₅-ZnO_{0.5}, there were virtually less colonies formation in the area in the presence of the composite films, while no growth of bacteria was observed when covered with the composite film of CNF₁₅/SL₄-ZnO_{0.5}. SEM images of MRSA on the composite films were also recorded. As shown in Figures S2B and S2C, there was marked difference in the amount of visualized bacteria in the presence of composite films as compared with that in the control group, which was likely due to the unfavorable attachment of bacteria on the smooth surface of composites. Notable, it was observed that the significant loss of bacteria growth was involved in the CNF₁₅/SL₄-ZnO_{0.5} and CNF₁₅-ZnO_{0.5}-treated samples. In addition, when bacteria treated with CNF₁₅/SL₄, the morphology of bacteria showed defined spherical-shaped with intact cell membrane exhibiting shrinkage to some extent. These observations may further support the notion that the addition of SL in the composite films may contribute to the enhanced antibacterial effect of ZnO NPs.

The antioxidant activities of films were evaluated based on the 2, 2-diphenyl-1-picrylhydrazyl (DPPH) free radical scavenging capacities. As shown in Figure S3A, the fabricated films containing SL exhibited higher DPPH free radical scavenging capacity compared to CNF or CNF₁₅-ZnO_{0.5}. Antioxidant activities of pure SL and ZnO NPs were also detected. As shown in Figure S3B, SL exhibited pronounced antioxidant activity while ZnO NPs showed almost no antioxidant activity, which suggested that SL could be used as antioxidant to improve the performance of composite films. At the similar concentration of SL, CNF₁₅/SL₄-ZnO_{0.5} (41.03 µg SL/mL) possessed weaker DPPH free radical scavenging capacity than that of pure SL (40 µg SL/mL). This observation might due to the higher accessibility of pure SL comparing to the SL captured in the composite film. Moreover, the gradual release of SL from the dense network structure of the films may lead to the decreased scavenging effect of the film. Based on these observations, it can be concluded that the incorporation of SL and ZnO NPs at a dosage of 200–400 µg/mL in the composite CNF₁₅/SL₄-ZnO_{0.5} contributed to the enhanced antibacterial and antioxidant activity of the film.

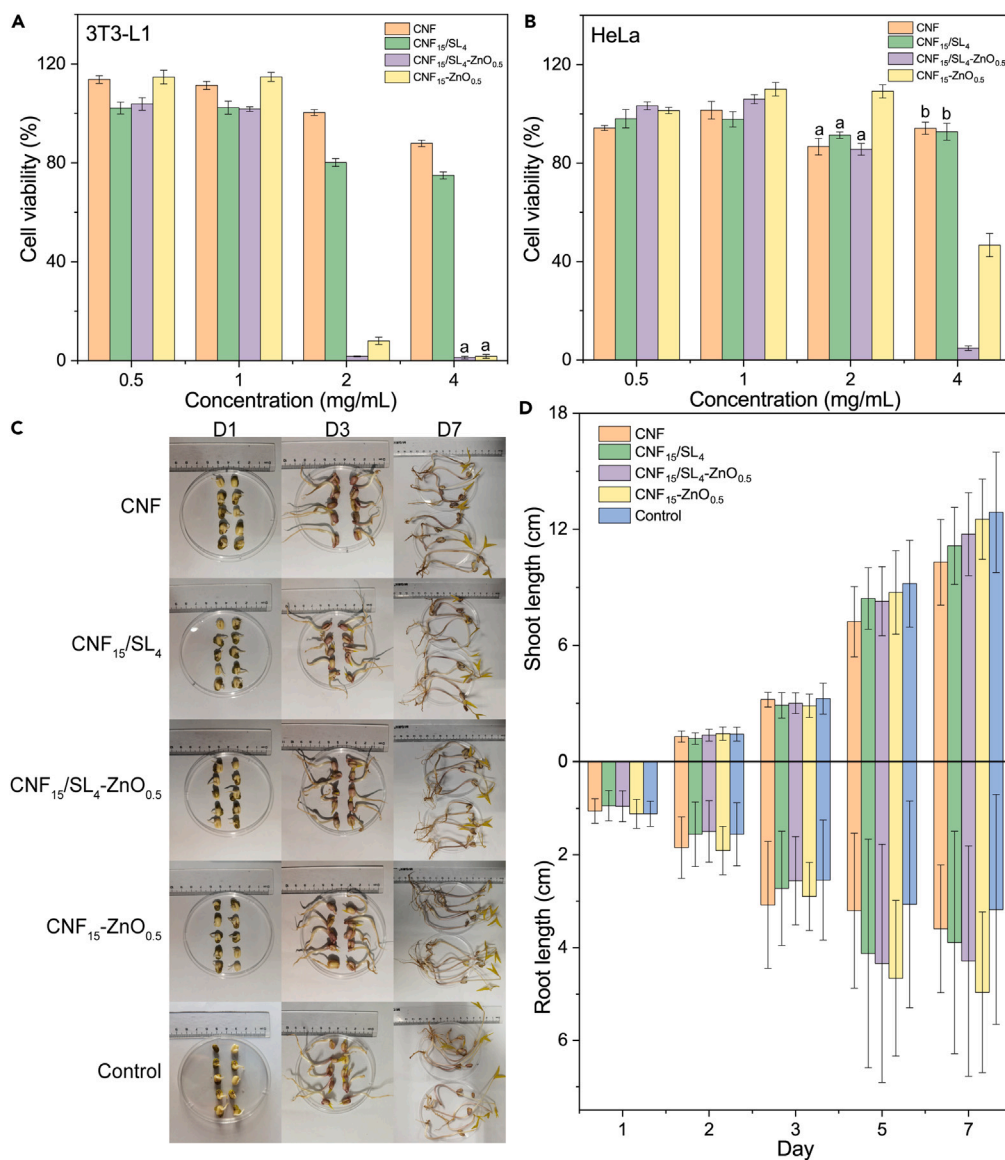


Figure 4. Cytotoxicity and phytotoxicity of composite films

(A and B) Viability of 3T3-L1 (A) and HeLa (B) exposed to different concentration of composite films.

(C and D) Representative images (C) and root and shoot length (D) of mung (*Vigna radiata*) after the treatment with different composite films. The same lowercase letters at the same sample concentration indicates no significant differences. Data are represented as mean \pm SD.

Biocompatibility evaluation

The biocompatibility of films is essential for practical uses. Hemolytic property, cytotoxicity, and phytotoxicity assays were performed to evaluate the biocompatibility of samples. As shown in Figure S4, the hemolytic properties of samples were examined using rat red blood cells (RBCs). Under the sample concentration ranging from 0.5–4 mg/mL that higher than the amount tested in antibacterial and antioxidant experiment, all prepared films exhibited no hemolytic activities (hemolysis <2%). The cytotoxicity evaluation was conducted using 3T3-L1 and HeLa cells after 24 h incubation with obtained materials (Figures 4A and 4B). It was found that no apparent cytotoxicity was observed up to 1 mg/mL (cell viability > 80%) and 3T3-L1 was more sensitive to materials compared to that of HeLa. Among four tested films, CNF₁₅/SL₄-ZnO_{0.5} possessed stronger cytotoxic effect at a high concentration (2 or 4 mg/mL), which was consistent with its superior antimicrobial activity.

The massive use of food packing films leading to the considerable accumulation of packaging waste, such as plastic films, has imposed serious impacts to the ecosystem. Therefore, it was necessary to study the potential risks caused by the disposal of films into the soil environment interacting with surrounding environmental components. Mung bean (*Vigna radiata*) is a legume crop recommended by the

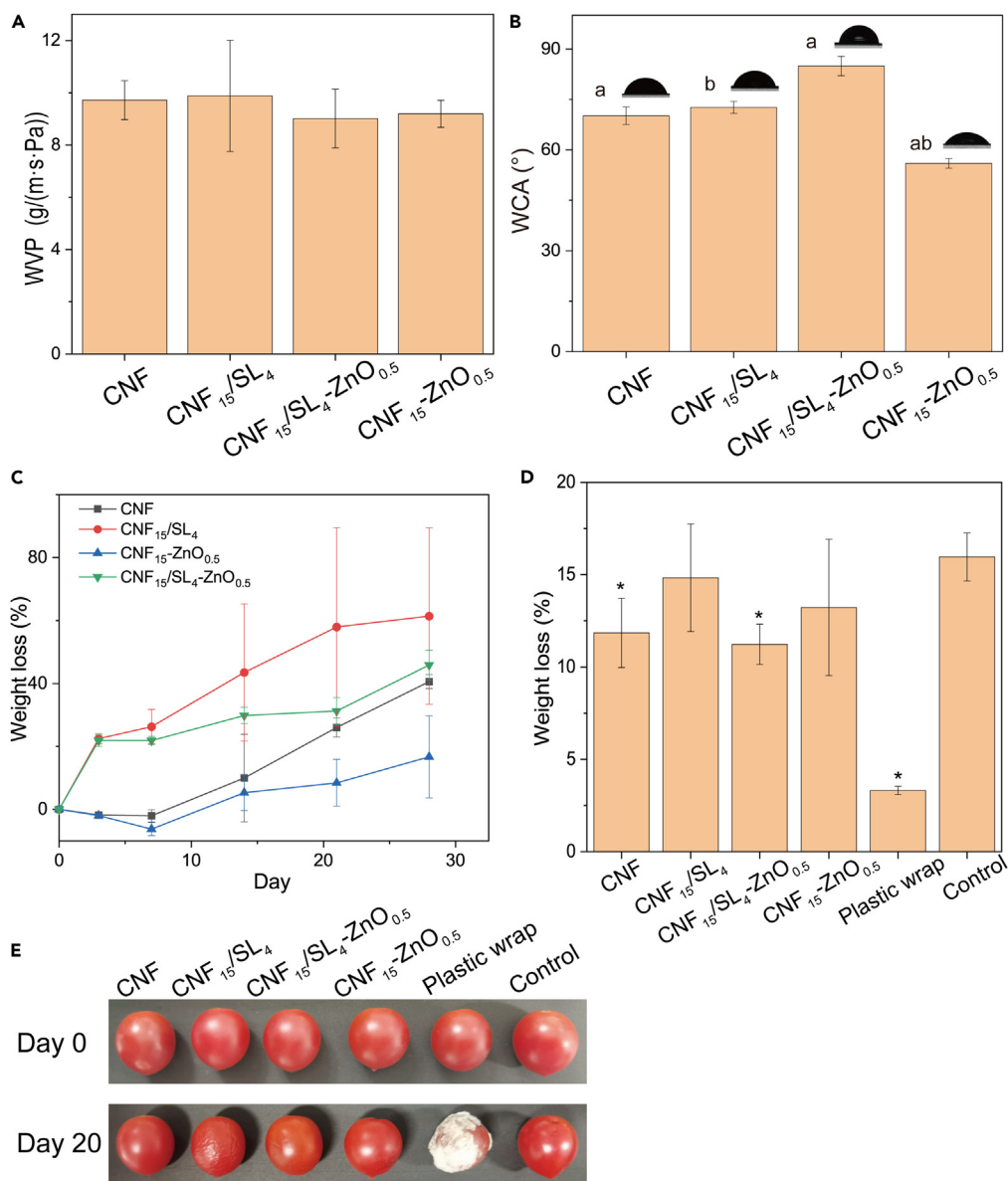


Figure 5. Evaluation of moisture barrier capability, hydrophobicity, biodegradability, and preservation performance of composite films

(A and B) Water vapor permeability (A) and surface water contact angle (B) of different composite films.

(C) Degradation of films in the soil during 28-day period.

(D and E) Weight loss (D) and representative images (E) of cherry tomatoes (*Lycopersicon esculentum* var. *cerasiforme*) preserved by different composite films and plastic wrap. Different lowercase letters in (B) indicates significant differences, while * in (D) indicates significant differences compared to the control group. Data are represented as mean \pm SD.

Organization for Economic Co-operation and Development (OECD) guidelines for terrestrial phytotoxicity test. The phytotoxicity of films was evaluated by germination rate and growth parameters including shoot and root length.^{35,36} The germination rates of mung beans untreated or treated with films were all 100%. Moreover, the growth of mung beans was not affected after the co-culture with different samples as the length of shoot and root showed no significant difference ($p > 0.05$) at 4 mg/mL concentration, indicating a negligible phytotoxicity of films involved (Figures 4C and 4D).

Moisture barrier property

The water vapor permeability (WVP) is a basic factor for the applications of films in food packaging, which is closely related to the porosity of the film matrix, surface hydrophobic structure, and hydrophilicity. As shown in Figure 5A, even though the WVP of synthesized films exhibited

no significant difference ($p > 0.05$), the WVP of CNF₁₅/SL₄-ZnO_{0.5} was relatively low, which may arise from the dense network formed by the three components.

Surface hydrophobicity

The water contact angle (WCA) was measured to evaluate the surface hydrophobicity. As shown in Figure 5B, all the films had the hydrophilic surface (WCA < 90°) due to the hydroxyl groups. The WCA of CNF₁₅-ZnO_{0.5} showed a decreased value, which may result from the increase of surface roughness due to the addition of ZnO NPs. Significant increase of WCA was observed for CNF₁₅/SL₄-ZnO_{0.5} with restricted water absorption tendency, which was attributed to the formation of the dense compact structure and more hydrogen bonds between the matrix and SL or ZnO NPs, and thereby inhibiting the interplay between the film and water molecules.²⁵ Additionally, the relatively large WCA measured for CNF₁₅/SL₄-ZnO_{0.5} confirmed its low WVP.

Biodegradability and food packaging

As the plastic pollution remains challenging issue for the eco-environmental protection, biodegradable packaging materials have increasing attentions. The biodegradability of the films was evaluated by the soil burial test. Figure 5C displayed the weight loss of films during 28 days experiment. The observable weight loss of CNF₁₅/SL₄ and CNF₁₅/SL₄-ZnO_{0.5} was the highest for the first three days, which was due to the shedding and decomposition of SL. After four weeks burial test, the percentage of weight loss of CNF, CNF₁₅/SL₄, CNF₁₅/SL₄-ZnO_{0.5}, and CNF₁₅-ZnO_{0.5} was measured to be 40.64%, 61.43%, 45.91%, and 16.69%, respectively. Considering that both lignin and cellulose were available carbon sources for soil microorganisms, it is reasonable that the CNF₁₅/SL₄ showed the highest degradation rate. Moreover, the reduction of weight loss of samples containing ZnO NPs compared to those films without ZnO NPs could be ascribed to the interference caused by the antimicrobial property of ZnO NPs on the enzymatic biodegradation of cellulose.

The preservation effect of prepared film was evaluated using cherry tomatoes (*Lycepersicon esculentum* var. *cerasiforme*) as model fruits. As shown in Figures 5D and 5E, the uncoated cherry tomato exhibited a withered shape due to the water evaporation after the preservation at 4°C for 20 days, the same as the CNF₁₅/SL₄ and CNF₁₅-ZnO_{0.5} group. Moreover, the weight loss rates of cherry tomatoes wrapped with CNF, CNF₁₅/SL₄-ZnO_{0.5}, and plastic wrap were significantly lower than those without film packaging. However, the excellent barrier property of plastic wrap may create a humid environment favorable for bacteria reproduce so that the tested cherry tomatoes more susceptible to spoilage and mildew. By comparison, the satisfied preservation effect of CNF₁₅/SL₄-ZnO_{0.5} was observed, which may benefit from the synergistic effect of the improved blocking properties (low WVP and high surface hydrophobicity) and antibacterial activities of the composite film to prevent the fruit from rotting. Based on these experimental observations, CNF₁₅/SL₄-ZnO_{0.5} represented promising potentials to replace plastic film as an alternative bio-based food packaging material.

Soil microbiota analysis

To further evaluate the effect of CNF₁₅/SL₄-ZnO_{0.5} degradation on soil environment, metagenome analysis was conducted to reveal the composition and function of microbial community in the soil before CNF₁₅/SL₄-ZnO_{0.5} degradation (W0) and after CNF₁₅/SL₄-ZnO_{0.5} degradation (W4). The Alpha diversity for W0 and W4 was evaluated through Chao1, Simpson, and Shannon index, which showed no significant changes between the two groups, indicating that the richness and evenness of soil microbial community were barely affected according to the degradation of the composite film (Figures S5A–S5C). Moreover, the distance value calculated using Euclidean distance exhibited no significant difference for the beta-diversity of two groups, reflecting a similar composition pattern of microbiota (Figure S5D).

Altogether, more than 4,800 species belonging to 4 kingdoms (bacteria, eukaryote, archaea, and viruses) were annotated for each sample. Figures 6A and 6B showed the composition of microbiota at phylum and genus level of all the samples. At phylum level, more than 45 phyla were annotated while the top 30 abundant phylum were listed on Figure 6A. When annotated at phylum level, the microorganisms in the soil were mainly members of Proteobacteria, Actinobacteria, Bacteroidetes, and Firmicutes belonging to bacteria kingdom, and Ascomycota belonging to eukaryote, which accounted for over 90% of the total sequences and was in accordance with previous reports.³⁷ As copiotrophs stimulated by increased nutrients in the environment, Proteobacteria of phylogenetic, pathogenic, and ecological significance played an important role in the decomposition of organic substances.³⁸ The second most dominant phylum, actinobacteria, had a strong metabolic capacity owing to their active DNA repair mechanism and Bacteroidetes have colonized across various ecological niches involving in carbon and nitrogen metabolism.^{37,39} The relative abundance of the top 30 genus only covered about 50% of the total sequences (Figure 6B). Difference in the soil microbiota between W0 and W4 was detected using linear discriminant analysis effect size (LEfSe) analysis. As shown in Figure 6C, the identified genus included *Bradyrhizobium*, *Rhizoiium*, *Mesorhizobium*, and *Cupriavidus*, which belonged to rhizobia known for fixing atmospheric nitrogen for host photosynthates and nodulating legume roots. Also, rhizobia were chemoheterotrophic bacteria that were unable to utilize cellulose or lignin.^{40,41} Moreover, genus *Streptomyces*, one of most abundant and important actinomycetes, was a major source of antibiotics.^{42,43} The abundance of genus *Streptomyces* was relatively high in W0 may be due to the release of ZnO NPs from the CNF₁₅/SL₄-ZnO_{0.5}, which inhibited the bacteria growth and reduced the production of antibiotics. Another plausible explanation was that *Streptomyces* were migrated and attached strongly to the surface of films instead of soil particles using their filaments for sporulation.⁴² W4 was rich in genus *Sphingomonas* and *Rhodococcus* that naturally degrade lignin and/or metabolize aromatics.⁴⁴ Genus *Rhodococcus*, a group of Gram-positive bacteria with diverse catabolic and adaptive capabilities for lignocellulosic biomass conversion were enriched in W4.⁴⁵

Further study on the function annotation of genes was conducted on Kyoto Encyclopedia of Genes and Genomes (KEGG) database, Comprehensive Antibiotic Resistance Database (CARD), and carbohydrate-active enzymes database (CAZY). Among all function annotations,

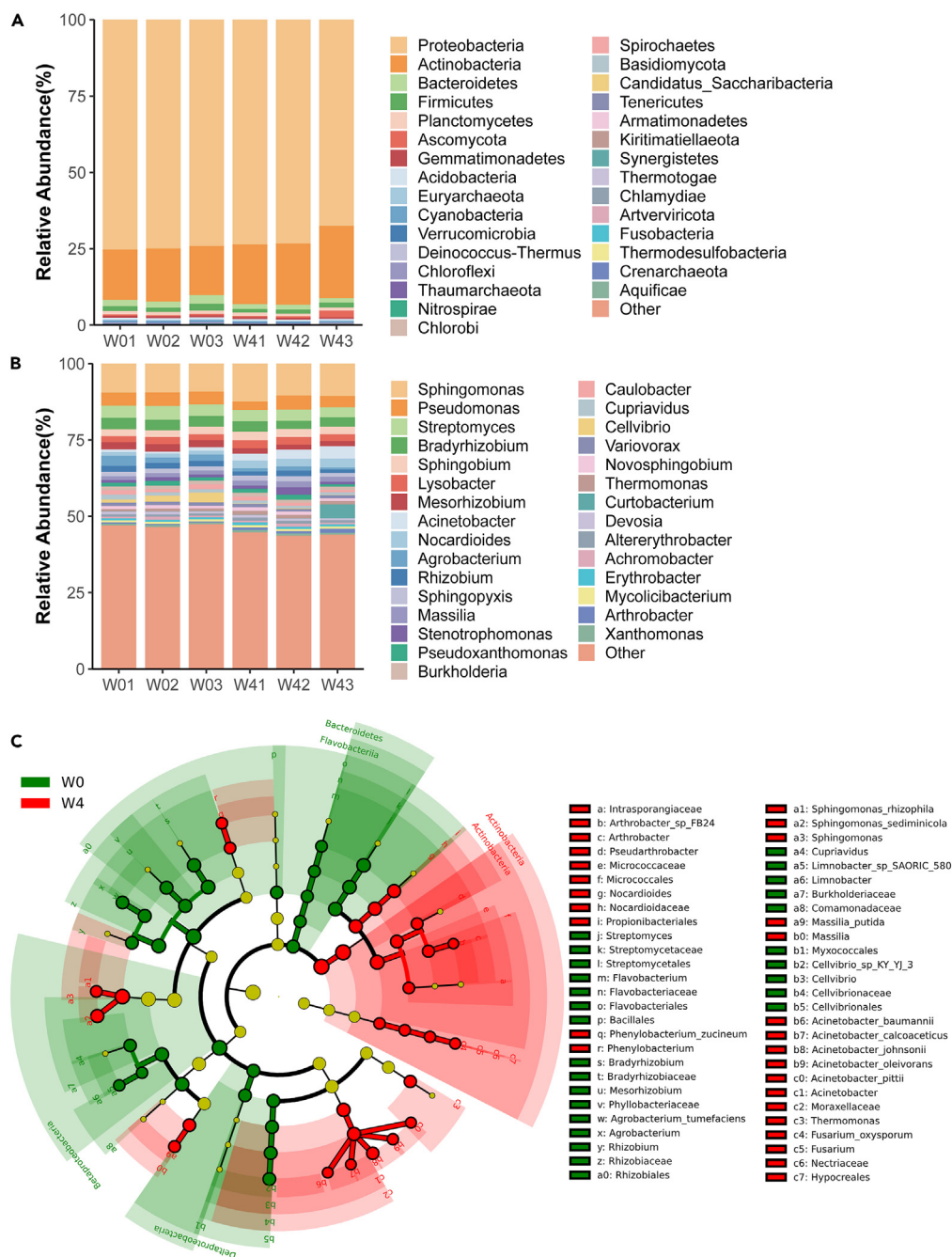


Figure 6. Composition of soil microbiota before and after film degradation

(A and B) Composition of microbiota at phylum (A) and genus (B) level.

(C) Cladogram of species annotated in soil samples. Clades significantly enriched in each cohort are indicated by the colors shown in the legend (LEfSe; linear discriminant analysis [LDA], log score > 2.0, $p = 0.05$). W0: before degradation; W4: after 4-week composite film degradation.

no significant intergroup change was observed, indicating a minimized damage involved in the film degradation. As shown in Figure 7A, the annotated KEGG secondary pathways were listed with corresponding number of genes classified by group. The chord diagrams were used to display the function classification in CARD (Figure 7B) and CAZy at level 2 (Figure 7C). CARD, including 322,710 unique ARG allele sequences, provides an informatics framework for resistomes annotation and interpretation, combining the antibiotic resistance ontology (ARO) with curated AMR gene (ARG) sequences and resistance-conferring mutations.⁴⁶ The total portion of W0 was higher than W4 which was displayed by the width of corresponding arc, indicating that the degradation of CNF₁₅/SL₄-ZnO_{0.5} caused no apparent increase of antibiotic resistance.

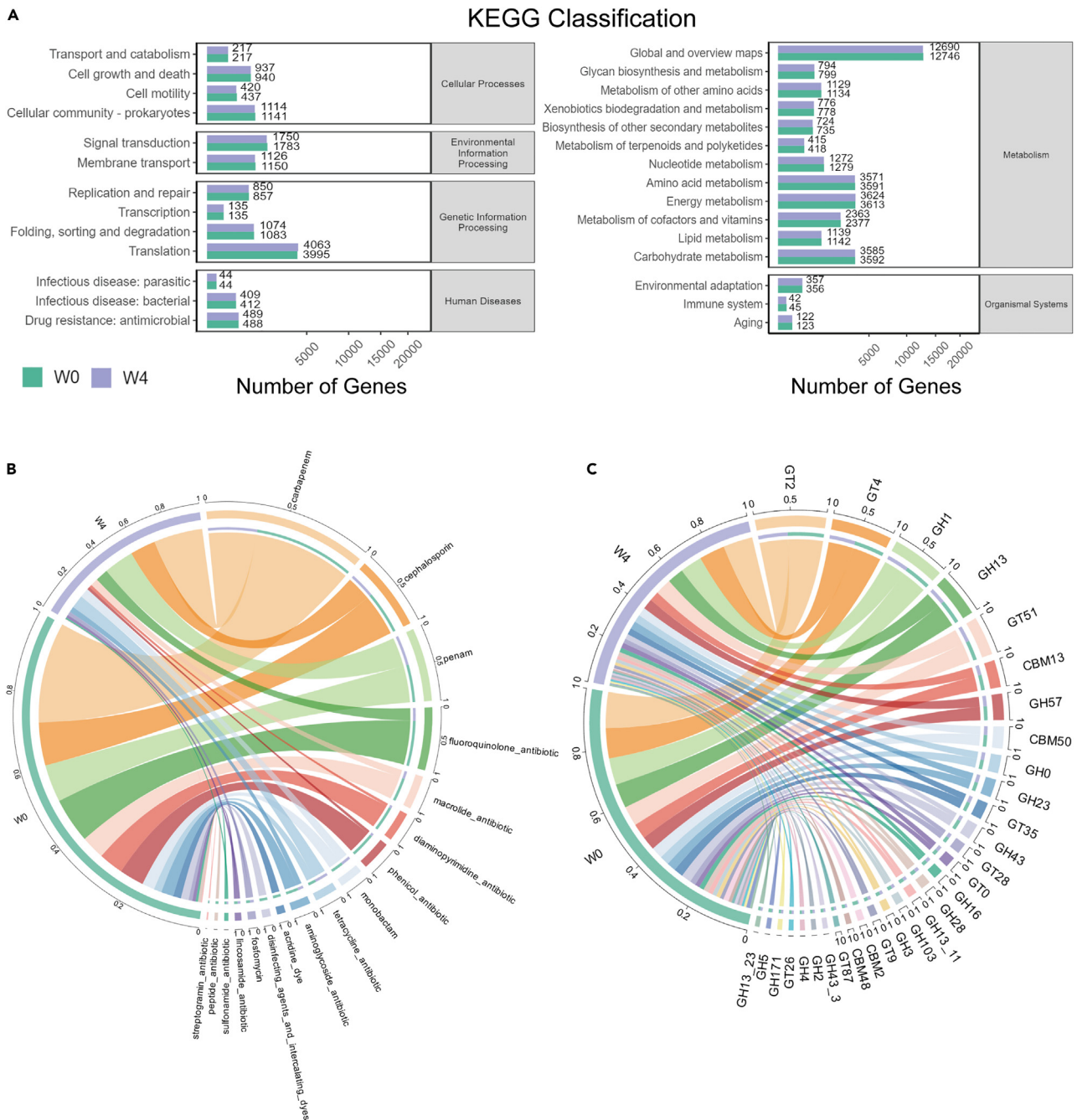


Figure 7. Function analysis of soil microbiota before and after film degradation

(A) The KEGG function classification analysis.

(B and C) The chord diagram of function classification annotated in Comprehensive Antibiotic Resistance Database (CARD) (B) and carbohydrate-active enzymes database (CAZy) at level 2 (C). W0: before degradation; W4: after 4-week composite film degradation.

The genes annotated at carbapenem, cephalosporin, macrolide, diaminopyrimidine, and phenicol antibiotic were less in W4 than W0, which could perhaps relate to the reduced abundance of *Streptomyces*. CAZy, a database specialized in the enzymes that build and breakdown complex carbohydrates and glycoconjugates, was classified as: glycoside hydrolases (GHs), glycosyltransferases (GTs), polysaccharide lyases (PLs), carbohydrate esterases (CEs), and carbohydrate-binding modules (CBMs).⁴⁷ Annotated at level 2, top 5 belonged to GHs or GTs. And the representative enzymes for GT2, GT4, and GH3 were cellulose synthase, sucrose synthase, and glucosidase which enabled the degradation and reuse of cellulose and lignin from the composite film.

DISCUSSION

Nowadays, foodborne pathogens remain a concerning issue for the public health, which urges considerable efforts of using eco-friendly materials for multifunctional food packaging including antibacterial, biocompatible and biodegradable properties. In this study, films composed with CNFs, SL, and ZnO NPs were successfully obtained. As characterized by a set of physicochemical experiments, the fabricated films possessed dense network structure, considerable mechanical properties, as well as good thermal stability and compatibility among all the components. The addition of SL and ZnO NPs provided UV-light protection, antimicrobial, and antioxidant properties. Moreover, the composite films were tested for the preservation of cherry tomatoes, which exhibited good moisture barrier capability and prolonged food shelf-life. Hemolysis, cytotoxicity and phytotoxicity evaluations of prepared films demonstrated a desirable biocompatibility of product. The superior biodegradability of the composed films was verified by the soil burial test and further evaluation on the composition and function of soil microbiota revealed no significant change was caused by the film decomposition.⁴⁸ Therefore, the constructed composite film of cellulose-lignin-ZnO NPs has provided a novel scheme for the design of high-performance antibacterial and biodegradable packaging materials in the substitution of non-degradable petroleum-based polymers, which is of practical importance for sustainable uses.^{49,50}

Limitations of the study

The current study has focused on sustainable resources for food packaging in the replacement of plastics, which revealed that cellulose-lignin-ZnO NPs composed film was a promising substitute of petroleum-based polymers. Nevertheless, the detailed structure-function relationship of constructed composite film as well as associated molecular mechanism remained to be clarified which is essential for the large-scale manufacture.

STAR★METHODS

Detailed methods are provided in the online version of this paper and include the following:

- KEY RESOURCES TABLE
- RESOURCE AVAILABILITY
 - Lead contact
 - Materials availability
 - Data and code availability
- EXPERIMENTAL MODEL AND STUDY PARTICIPANT DETAILS
 - Microbe strains
 - Cell lines and cell culture
- METHOD DETAILS
 - Synthesis of ZnO nanoparticles
 - Preparation of the composite films
 - Characterization of the films
 - Antibacterial activities
 - Antioxidant activities
 - Biocompatibility evaluation
 - Water vapor permeability
 - Water contact angle
 - Biodegradability test
 - Food preservation test
 - Soil microbiota analysis
 - Statistical analysis

SUPPLEMENTAL INFORMATION

Supplemental information can be found online at <https://doi.org/10.1016/j.isci.2024.110008>.

ACKNOWLEDGMENTS

The study was supported by Natural Science Foundation of Jiangsu Higher Education Institutions of China (No. 23KJA330001), Foundation of Chongqing Key Laboratory of Prevention and Treatment for Occupational Diseases and Poisoning (Grant No. 2022-2023ZYBK05) and a project funded by the Priority Academic Program Development of Jiangsu Higher Education Institutions (PAPD) for financial support.

AUTHOR CONTRIBUTIONS

X.Z., conceptualization, methodology, investigation, and writing – original draft. H.L., methodology, investigation, and writing – original draft. L.C., investigation. Y.W., investigation. J.W., writing – review & editing and project administration. S.X., writing – review & editing and project

administration. S.W., methodology and project administration. H.W., methodology. D.W., writing – review & editing. J.C., supervision, conceptualization, project administration, and writing – review & editing.

DECLARATION OF INTERESTS

The authors declare no competing interest.

Received: September 14, 2023

Revised: March 1, 2024

Accepted: May 14, 2024

Published: May 16, 2024

REFERENCES

- Halloub, A., Raji, M., Essabir, H., Chakchak, H., Boussen, R., Bensalah, M.O., Bouhfid, R., and Qaiss, A.E.K. (2022). Intelligent food packaging film containing lignin and cellulose nanocrystals for shelf life extension of food. *Carbohydr. Polym.* 296, 119972.
- Lai, W.F., Zhao, S., and Chiou, J. (2021). Antibacterial and clusteroluminogenic hypromellose-graft-chitosan-based polyelectrolyte complex films with high functional flexibility for food packaging. *Carbohydr. Polym.* 271, 118447.
- Barone, A.S., Matheus, J.R.V., de Souza, T.S.P., Moreira, R.F.A., and Fai, A.E.C. (2021). Green-based active packaging: Opportunities beyond COVID-19, food applications, and perspectives in circular economy-A brief review. *Compr. Rev. Food Sci. Food Saf.* 20, 4881–4905.
- Oliveira, W.Q.d., Azeredo, H.M.C.d., Neri-Numa, I.A., and Pastore, G.M. (2021). Food packaging wastes amid the COVID-19 pandemic: Trends and challenges. *Trends Food Sci. Technol.* 116, 1195–1199.
- Asgher, M., Qamar, S.A., Bilal, M., and Iqbal, H.M.N. (2020). Bio-based active food packaging materials: Sustainable alternative to conventional petrochemical-based packaging materials. *Food Res. Int.* 137, 109625.
- (2018). The future of plastic. *Nat. Commun.* 9, 2157.
- Stephanie, B., Borrelle, J.R., Lavender Law, K., Monahan, C.C., Lebreton, L., McGivern, A., Murphy, E., Jambeck, J., Leonard, G.H., Hilleary, M.A., et al. (2020). Predicted growth in plastic waste exceeds efforts to mitigate plastic pollution. *Science* 369, 1515–1518.
- Horton, A.A. (2022). Plastic pollution: When do we know enough? *J. Hazard Mater.* 422, 126885.
- Su, Z., Huang, S., Wang, Y., Ling, H., Yang, X., Jin, Y., Wang, X., and Zhang, W. (2020). Robust, high-barrier, and fully recyclable cellulose-based plastic replacement enabled by a dynamic imine polymer. *J. Mater. Chem. A Mater.* 8, 14082–14090.
- Ahari, H., Golestan, L., Anvar, S.A.A., Cacciotti, I., Garavand, F., Rezaei, A., Sani, M.A., and Jafari, S.M. (2022). Bio-nanocomposites as food packaging materials; the main production techniques and analytical parameters. *Adv. Colloid Interface Sci.* 310, 102806.
- Li, X., Ren, Z., Wang, R., Liu, L., Zhang, J., Ma, F., Khan, M.Z.H., Zhao, D., and Liu, X. (2021). Characterization and antibacterial activity of edible films based on carboxymethyl cellulose, *Dioscorea opposita* mucilage, glycerol and ZnO nanoparticles. *Food Chem.* 349, 129208.
- Oun, A.A., Shankar, S., and Rhim, J.W. (2020). Multifunctional nanocellulose/metal and metal oxide nanoparticle hybrid nanomaterials. *Crit. Rev. Food Sci. Nutr.* 60, 435–460.
- Wang, X., Xia, Q., Jing, S., Li, C., Chen, Q., Chen, B., Pang, Z., Jiang, B., Gan, W., Chen, G., et al. (2021). Strong, Hydrostable, and Degradable Straws Based on Cellulose-Lignin Reinforced Composites. *Small* 17, e2008011.
- Crowther, T.W., Glick, H.B., Covey, K.R., Bettigole, C., Maynard, D.S., Thomas, S.M., Smith, J.R., Hintler, G., Duguid, M.C., Amatulli, G., et al. (2015). Mapping tree density at a global scale. *Nature* 525, 201–205.
- Rossi, B.R., Pellegrini, V.O.A., Cortez, A.A., Chiromito, E.M.S., Carvalho, A.J.F., Pinto, L.O., Rezende, C.A., Mastelaro, V.R., and Polikarpov, I. (2021). Cellulose nanofibers production using a set of recombinant enzymes. *Carbohydr. Polym.* 256, 117510.
- Roy, S., and Rhim, J.W. (2020). Carboxymethyl cellulose-based antioxidant and antimicrobial active packaging film incorporated with curcumin and zinc oxide. *Int. J. Biol. Macromol.* 148, 666–676.
- Rana, A.K., Frollini, E., and Thakur, V.K. (2021). Cellulose nanocrystals: Pretreatments, preparation strategies, and surface functionalization. *Int. J. Biol. Macromol.* 182, 1554–1581.
- An, L., Chen, J., Heo, J.W., Bae, J.H., Jeong, H., and Kim, Y.S. (2021). Synthesis of lignin-modified cellulose nanocrystals with antioxidant activity via Diels-Alder reaction and its application in carboxymethyl cellulose film. *Carbohydr. Polym.* 274, 118651.
- Melro, E., Alves, L., Antunes, F.E., and Medronho, B. (2018). A brief overview on lignin dissolution. *J. Mol. Liq.* 265, 578–584.
- Dominguez-Robles, J., Larraneta, E., Fong, M.L., Martin, N.K., Irwin, N.J., Mutje, P., Tarres, Q., and Delgado-Aguilar, M. (2020). Lignin/poly(butylene succinate) composites with antioxidant and antibacterial properties for potential biomedical applications. *Int. J. Biol. Macromol.* 145, 92–99.
- Ma, L., Zhu, Y., Huang, Y., Zhang, L., and Wang, Z. (2022). Strong water-resistant, UV-blocking cellulose/glucomannan/lignin composite films inspired by natural LCC bonds. *Carbohydr. Polym.* 281, 119083.
- Cassales, A., Ramos, L.A., and Frollini, E. (2020). Synthesis of bio-based polyurethanes from Kraft lignin and castor oil with simultaneous film formation. *Int. J. Biol. Macromol.* 145, 28–41.
- Weiland, F., Kohlsted, M., and Wittmann, C. (2022). Guiding stars to the field of dreams: Metabolically engineered pathways and microbial platforms for a sustainable lignin-based industry. *Metab. Eng.* 71, 13–41.
- Al-Tayyar, N.A., Youssef, A.M., and Al-Hindi, R. (2020). Antimicrobial food packaging based on sustainable Bio-based materials for reducing foodborne Pathogens: A review. *Food Chem.* 310, 125915.
- Xie, Y., Pan, Y., and Cai, P. (2022). Cellulose-based antimicrobial films incorporated with ZnO nanoparticles on surface as biodegradable and antimicrobial packaging. *Food Chem.* 368, 130784.
- Mishra, P.K., Mishra, H., Ekielski, A., Talegaonkar, S., and Vaidya, B. (2017). Zinc oxide nanoparticles: a promising nanomaterial for biomedical applications. *Drug Discov. Today* 22, 1825–1834.
- Xie, Y., He, Y., Irwin, P.L., Jin, T., and Shi, X. (2011). Antibacterial activity and mechanism of action of zinc oxide nanoparticles against *Campylobacter jejuni*. *Appl. Environ. Microbiol.* 77, 2325–2331.
- Kim, H.-J., Roy, S., and Rhim, J.-W. (2022). Gelatin/agar-based color-indicator film integrated with *Clitoria ternatea* flower anthocyanin and zinc oxide nanoparticles for monitoring freshness of shrimp. *Food Hydrocolloids* 124, 107294.
- Pirnia, M., Shirani, K., Tabatabaee Yazdi, F., Moratazavi, S.A., and Mohebbi, M. (2022). Characterization of antioxidant active biopolymer bilayer film based on gelatin-frankincense incorporated with ascorbic acid and *Hyssopus officinalis* essential oil. *Food Chem. X* 14, 100300.
- Zhu, J., Gao, W., Wang, B., Kang, X., Liu, P., Cui, B., and Abd El-Aty, A.M. (2021). Preparation and evaluation of starch-based extrusion-blown nanocomposite films incorporated with nano-ZnO and nano-SiO₂. *Int. J. Biol. Macromol.* 183, 1371–1378.
- Liang, J., Ning, R., Sun, Z., Liu, X., Sun, W., and Zhou, X. (2021). Preparation and characterization of an eco-friendly dust suppression and sand-fixation liquid mulching film. *Carbohydr. Polym.* 256, 117429.
- Michelin, M., Marques, A.M., Pastrana, L.M., Teixeira, J.A., and Cerqueira, M.A. (2020). Carboxymethyl cellulose-based films: Effect of organosolv lignin incorporation on physicochemical and antioxidant properties. *J. Food Eng.* 285, 110107.
- Wang, C., Chang, T., Dong, S., Zhang, D., Ma, C., Chen, S., and Li, H. (2020). Biopolymer

- films based on chitosan/potato protein/linseed oil/ZnO NPs to maintain the storage quality of raw meat. *Food Chem.* 332, 127375.
34. Yu, F., Fei, X., He, Y., and Li, H. (2021). Poly(lactic acid)-based composite film reinforced with acetylated cellulose nanocrystals and ZnO nanoparticles for active food packaging. *Int. J. Biol. Macromol.* 186, 770–779.
 35. Leopold, L.F., Coman, C., Clapa, D., Oprea, I., Toma, A., Iancu, Ș.D., Barbu-Tudoran, L., Suci, M., Ciorîță, A., Cadiș, A.I., et al. (2022). The effect of 100–200 nm ZnO and TiO₂ nanoparticles on the in vitro-grown soybean plants. *Colloids Surf. B Biointerfaces* 216, 112536.
 36. Sun, Y., Wang, W., Zheng, F., Zhang, S., Wang, F., and Liu, S. (2020). Phytotoxicity of iron-based materials in mung bean: Seed germination tests. *Chemosphere* 251, 126432.
 37. Wang, X., Zhang, Z., Yu, Z., Shen, G., Cheng, H., and Tao, S. (2020). Composition and diversity of soil microbial communities in the alpine wetland and alpine forest ecosystems on the Tibetan Plateau. *Sci. Total Environ.* 747, 141358.
 38. Mundra, S., Kjønaas, O.J., Morgado, L.N., Krabberød, A.K., Ransedokken, Y., and Kauserud, H. (2021). Soil depth matters: shift in composition and inter-kingdom co-occurrence patterns of microorganisms in forest soils. *FEMS Microbiol. Ecol.* 97, fiab022.
 39. Sarah Stewart Johnson, M.B.H., Christensen, T.R., Mastepanov, M., Nielsen, R., Munch, K., Brand, T., Gilbert, M.T.P., Zuber, M.T., Bunce, M., Rønn, R., et al. (2007). Ancient bacteria show evidence of DNA repair. *Proc. Natl. Acad. Sci. USA* 104, 14401–14405.
 40. Gano-Cohen, K.A., Stokes, P.J., Blanton, M.A., Wendlandt, C.E., Hollowell, A.C., Regus, J.U., Kim, D., Patel, S., Pahua, V.J., and Sachs, J.L. (2016). Nonnodulating Bradyrhizobium spp. Modulate the Benefits of Legume-Rhizobium Mutualism. *Appl. Environ. Microbiol.* 82, 5259–5268.
 41. Liang, Y., and Yu, H. (2021). Genetic toolkits for engineering Rhodococcus species with versatile applications. *Biotechnol. Adv.* 49, 107748.
 42. Olanrewaju, O.S., and Babalola, O.O. (2019). Streptomyces: implications and interactions in plant growth promotion. *Appl. Microbiol. Biotechnol.* 103, 1179–1188.
 43. Worrall, J.A.R., and Vijgenboom, E. (2010). Copper mining in Streptomyces: enzymes, natural products and development. *Nat. Prod. Rep.* 27, 742–756.
 44. Mních, E., Vanholme, R., Oyarce, P., Liu, S., Lu, F., Goeminne, G., Jørgensen, B., Motawie, M.S., Boerjan, W., Ralph, J., et al. (2017). Degradation of lignin beta-aryl ether units in Arabidopsis thaliana expressing LigD, LigF and LigG from Sphingomonas paucimobilis SYK-6. *Plant Biotechnol. J.* 15, 581–593.
 45. Rosnow, J.J., Anderson, L.N., Nair, R.N., Baker, E.S., and Wright, A.T. (2017). Profiling microbial lignocellulose degradation and utilization by emergent omics technologies. *Crit. Rev. Biotechnol.* 37, 626–640.
 46. Alcock, B.P., Huynh, W., Chalil, R., Smith, K.W., Raphenya, A.R., Wlodarski, M.A., Edalatmand, A., Petkau, A., Syed, S.A., Tsang, K.K., et al. (2023). CARD 2023: expanded curation, support for machine learning, and resistome prediction at the Comprehensive Antibiotic Resistance Database. *Nucleic Acids Res.* 51, D690–D699.
 47. Cantarel, B.L., Coutinho, P.M., Rancurel, C., Bernard, T., Lombard, V., and Henrissat, B. (2009). The Carbohydrate-Active EnZymes database (CAZy): an expert resource for Glycogenomics. *Nucleic Acids Res.* 37, D233–D238.
 48. Wei, S., Ma, J.-X., Xu, L., Gu, X.-S., and Ma, X.-L. (2020). Biodegradable materials for bone defect repair. *Mil. Med. Res.* 7, 54.
 49. Murray, R.Z., West, Z.E., Cowin, A.J., and Farrugia, B.L. (2019). Development and use of biomaterials as wound healing therapies. *Burns Trauma* 7, 2.
 50. Chen, Z., Wei, W., Chen, H., and Ni, B.-J. (2022). Recent advances in waste-derived functional materials for wastewater remediation. *Eco. Environ. Health* 1, 86–104.
 51. Zhu, X., Li, H., Zhou, L., Jiang, H., Ji, M., and Chen, J. (2023). Evaluation of the gut microbiome alterations in healthy rats after dietary exposure to different synthetic ZnO nanoparticles. *Life Sci.* 312, 121250.
 52. Zhu, X., Wang, J., Cai, L., Wu, Y., Ji, M., Jiang, H., and Chen, J. (2022). Dissection of the antibacterial mechanism of zinc oxide nanoparticles with manipulable nanoscale morphologies. *J. Hazard Mater.* 430, 128436.

STAR★METHODS

KEY RESOURCES TABLE

REAGENT or RESOURCE	SOURCE	IDENTIFIER
Bacterial and virus strains		
<i>Escherichia coli</i>	ATCC	ATCC 25922
<i>Staphylococcus aureus</i>	ATCC	ATCC 6538
methicillin-resistant <i>Staphylococcus aureus</i>	ATCC	ATCC 433600
Chemicals, peptides, and recombinant proteins		
Cellulose nanofibers	Qihong Scientific	N/A
Sodium lignosulfonate	Macklin	Cat# S817764
2, 2-Diphenyl-1-picrylhydrazyl (DPPH)	Macklin	Cat# D807297
Zn(acac) ₂	Tokyo Kasei Kogyo	Cat# Z0002
Polyethylene glycol (PEG) with Mn of 1000 (95%)	Xilong Chemistry	Cat# 12803702
Critical commercial assays		
Cell Counting Kit-8	MedChemExpress	Cat# HY-K0301
Deposited data		
Raw paired-end reads of metagenome analysis of soil samples	This paper	SRA NCBI: PRJNA983264
Experimental models: Cell lines		
HeLa	ATCC	N/A
3T3-L1	ATCC	N/A
Software and algorithms		
Origin	OriginLab	https://www.originlab.com/
SPSS 18.0	IBM	https://www.ibm.com/spss
MEGAHIT	N/A	https://github.com/voutcn/megahit
R	The R foundation	https://www.R-project.org
MetaGeneMark	N/A	http://topaz.gatech.edu/GeneMark/license_download.cgi
Cd-hit	N/A	https://github.com/weizhongli/cdhit/archive/V4.6.2.tar.gz

RESOURCE AVAILABILITY

Lead contact

Requests for information and resources should be directed to the lead contact, Prof. Jin Chen (okachen30@gmail.com or jchen@njmu.edu.cn).

Materials availability

This study did not generate any new unique reagents.

Data and code availability

- The study has not been preregistered.
- All data reported in this paper will be shared by the [lead contact](#) upon request.
- This paper does not report original code.
- Raw paired-end reads of metagenome analysis of soil microbiota were deposited into the Sequence Read Archive (SRA) of the NCBI and are publicly available as of the date of publication. Accession number is listed in the [key resources table](#).
- Any additional information required to re-analyze the data reported in this paper is available from the [lead contact](#) upon request.

EXPERIMENTAL MODEL AND STUDY PARTICIPANT DETAILS

Microbe strains

Microbe strains were purchased from American Type Culture Collection (ATCC, USA). Gram-negative *Escherichia coli* (*E. coli*, ATCC 25922) and Gram-positive *Staphylococcus aureus* (*S. aureus*, ATCC 6538) and MRSA (ATCC 43300) were chosen as model bacteria for the *in vitro* antibacterial activity through spread plate method. The bacteria were cultured in Luria-Bertani (LB) broth at 37°C

Cell lines and cell culture

Cells were purchased from ATCC. Human cervical cancer cells (HeLa) and mouse embryo fibroblasts (3T3-L1) were cultured in DMEM (Gibco) supplemented with 10% (v/v) fetal bovine serum (FBS, ExCell Biology) and 1% (v/v) penicillin–streptomycin (Gibco) in a humidified 5% CO₂ atmosphere at 37°C.

METHOD DETAILS

Synthesis of ZnO nanoparticles

The synthesis of ZnO NPs was following our previous reports with modifications.⁵¹ Briefly, the PEG 1000 (150 g) was added in a three-necked, round-bottomed flask and magnetically stirred for 30 min at 90°C. Then 5.3 g Zn(acac)₂ was added followed with another 20 min stirring and the gradual heating to 260°C. The reaction continued for 2 h under nitrogen stream (0.2 L/min) resulting in the formation of PEG capped ZnO NPs and the mixture was cooled to 80°C. The collected samples were washed with toluene and acetone to remove excessive PEG 1000 to obtain the final product of ZnO NPs by centrifugation.

Preparation of the composite films

The fabrication of the films was using a solution casting method. Firstly, 0.3 g of CNF was dispersed in 40 mL of deionized water on a 2000 rpm magnetic stirrer and remained stirring for 12 min at room temperature. Then SL and ZnO NPs were added and stirred for another 2 min. Ultrasonic was used for the mixture for degassing. The degassed solution was casted on a container (13.5 × 10.5 × 5.5 cm) to form the film and put in an oven at 160°C for 7 h. The film was peeled and maintained for further use. The films were designated according to the type of filler and the specified material ratios were listed in [Table S1](#).

Characterization of the films

Scanning electron microscopy (SEM, JEOL JSM-7900F, Japan) was used to monitor the surface morphology of the films. The samples were coated with Au/Pd prior to testing. The thickness of the composed films was obtained by a digital micrometer (Syntec Electro Tech Co. Ltd., China) to the nearest 0.001 mm. The mechanical properties (TS, EB) of the films were tested using a universal mechanical testing machine (AGS-X-50N, Shimadzu, Japan). FTIR-ATR spectra of films were measured using an FTIR Spectrometer (Thermo Scientific Nicolet Is20, USA) with a wavelength range of 4000–400 cm⁻¹. The scanning resolution and the number of cumulative scans were set as 4 cm⁻¹ and 32, respectively. The thermal stabilities of the films were determined using a thermogravimetric analyzer (STA 449 F5, Netzsch, German) from 30 to 800°C at 10°C/min heating rate under a nitrogen atmosphere. The UV-vis diffuse reflectance spectra were determined by a UV-visible spectrophotometer (UV-3600, Shimadzu, Japan) in the wavelength of 200–800 nm.

Antibacterial activities

The bacteria were cultured in Luria-Bertani (LB) broth at 37°C and 220 rpm until the concentration was 10⁸ CFU/mL (measured by the OD₆₀₀) for further assay. The bacteria were collected after washing with saline buffer and centrifuged for 3 times, and finally resuspended in saline buffer.

The composite films were cut and sterilized with ultraviolet light for 30 min first and then dissolved in saline water, mixing with bacteria suspension where the final concentration of bacteria was 10⁶ CFU/mL while the composite films concentrations were 200 and 400 μg/mL. Then the mixtures were incubated in the shaker, and 100 μL solution was taken out after 4 h and 16 h incubation, respectively and spread evenly on an agar plate and incubated at 37°C.

In order to further evaluate the bacteria growth on the surface of the film, agar diffusion assay was adopted. Specifically, the composite films were trimmed into a circle shape with a diameter of 1.3 cm and sterilized with 30 min ultraviolet. 100 μL 10⁶ CFU/mL MRSA solution was applied evenly on the agar plate with the samples placed on the center of the plate. Incubated at 37°C for 16 h, the bacteria growth was observed and photos were taken for each plate.

As for the SEM observation, 500 μL MRSA (10⁷ CFU/mL) in LB culture medium was incubated with UV-sterilized square composite film (length of side: 1.5 cm) in a 12-well plate for 4 h and 300 μL LB culture medium was supplemented every 30 min to prevent bacterial death caused by drying of the bacterial solution. After incubation, films were carefully rinsed 3 times with PBS for further fixation. 10 μL MRSA suspension added on a clean silicon chip followed by naturally air-drying was set as the control group. All the tested samples were fixed overnight with 2.5% glutaraldehyde at 4°C followed with the glutaraldehyde sucked, rinsed with PBS for 3 times, and finally dehydrated with ethanol. After natural air drying, samples were coated with Au/Pd prior to testing.

Antioxidant activities

The DPPH radical scavenging assay was performed to study the antioxidant activity of composed films, pure SL and ZnO NPs. Briefly, materials were suspended in deionized water and added with 200 $\mu\text{mol/L}$ DPPH ethanol solution, the mixtures were incubated at room temperature in the dark for 1 h, absorbance at 517 nm was measured using a multifunctional microplate reader (Tecan Infinite M200 Pro, Switzerland). De-ionized water added with DPPH solution was set as control. Scavenging activity (%) was calculated following equation:

$$\text{Scavenging activity (\%)} = \frac{(Abs_{control} - Abs_{sample})}{Abs_{control}} \times 100$$

The measurement was conducted in triplicate.

Biocompatibility evaluation

Hemolysis assay

Hemolysis assay was conducted following our previous report.⁵² Fresh RBCs were washed 3 times by PBS buffer following the steps of centrifuge and resuspension, and the suspension was diluted to approximate 4% (v/v) for further use. RBC suspension and pre-sterilized composite films immersed in PBS solution were mixed and the mixtures were incubated in 37°C for 1 h. The PBS buffer and 0.1% (v/v) Triton X-100 were used respectively as negative control and positive control. The supernatant was collected through centrifuge at 3000 rpm for 5 min, and 100 μL of each sample's supernatant was added into a 96-well plate for the continuous measurement of the sample absorbance at 570 nm on a multifunctional microplate reader (Tecan Infinite M200 Pro, Switzerland). The percentage of hemolysis was calculated as the following equation:

$$\text{Hemolysis (\%)} = \frac{Abs_{sample} - Abs_{NC}}{Abs_{PC} - Abs_{NC}} \times 100$$

The experiment was conducted in triplicate.

Cytotoxicity evaluation

Cell suspension was added to a 96-well plate with approximately 4000 cells per well. After 24 h incubation, the culture media was replaced by prearranged extract solution which was pre-prepared by soaking films into the DMEM medium at 37°C for 24 h before usage, and the plate were incubated for another 24 h. CCK-8 assay was conducted according to the manufacturer's protocol, the absorbance at 450 nm was recorded for samples, control and blank medium and cell viability was determined as the following equation:

$$\text{Cell viability (\%)} = \frac{Abs_{sample} - Abs_{blank}}{Abs_{control} - Abs_{blank}} \times 100$$

The experiment was proceeded triplicate.

Phytotoxicity evaluation

To investigate the effects of composite films on seed germination and growth for 7 days, the seeds of mung bean (*Vigna radiata*) were purchased and selected for healthy and intact seeds. Prior to the tests, the seeds were surface-sterilized with NaClO solution (0.5%) and washed with deionized water. 10 sterilized seeds were set evenly in each Petri dish (diameter:90 mm), added with 20 mg different film immersed in 5 mL water. The seeds were cultured in the dark at 25°C for 7 days to monitor germination, adding water when necessary. The roots and shoots length were measured at Day 1, 2, 3, 5, and 7.

Water vapor permeability

The WVP of films was measured according to previous reports with minor modifications. Briefly, the molecular sieve 10 \times , as water absorbent, was dried at 150°C oven for 24 h prior to the test. The dried absorbent was filled into 15 mL centrifuge tubes and the whole tubes were weighted as w_0 . The lids were replaced with the films and secured with rubber bands, placing at 23°C and 90% RH for 24 h. The weight of tubes was measured again as w_1 . WVP was calculated using the following formula:

$$\text{WVP (g / (m} \cdot \text{s} \cdot \text{Pa))} = \frac{(w_1 - w_0) \times L}{\Delta t \times A \times \Delta p}$$

where w_0 and w_1 were the weight of tubes before and after the experiment, and L and A were the thickness and effective coverage area of the tested films. Δt was the interval time, while Δp was the saturated vapor pressure of water at 23°C.

Water contact angle

The surface hydrophobicity of nanocomposite films was evaluated by measuring the WCA through a contact angle measuring instrument (OCA20, Dataphysics, Germany) equipped with a micro camera. A water droplet was applied to the film surface for 3 s before measurement.

Biodegradability test

Biodegradation test of films was carried out in soil conditions. The samples were cut into square (3 cm × 3 cm) and dried at 50°C to get initial weight. The films were placed on the soil and covered with a thin layer soil. The soil was put at room temperature and water was sprayed every 2–3 days. The degradation of films was monitored on Day 3, 7, 14, 21, and 28 by measuring the weight loss, and the whole experiment last for 28 days. The results were repeated three times. Soil samples at Day 0 and 28 were collected using sterilized 1.5 mL EP tubes and stored at –80°C for the further metagenome analysis.

Food preservation test

Cherry tomatoes (*Lycopersicon esculentum* var. *cerasiforme*) were used to investigate the food preservation ability. Fresh cherry tomatoes were collected and randomized to be wrapped with different films while the control group was directly exposed to air. The samples were stored at 4°C for 20 days. The food preservation ability was evaluated using a digital camera and measurement of weight loss of cherry tomatoes. Results were repeated three times.

Soil microbiota analysis

Metagenome analysis was used to evaluate the microbial composition of soil. All collected soil samples (W0 and W4 represented soil samples before and after CNF₁₅/SL₄-ZnO_{0.5} degradation) were sent to BGI Genomics Co., Ltd. (Shenzhen, China). Microbiome DNA was extracted and prepared to construct library, following the procedure of sample quality control, genomic DNA fragment, fragments selection, adaptor ligation, PCR, library quality control, circularization, and sequencing. All the raw data were trimmed to get high-quality reads which were further *de novo* assembled using MEGAHIT software. Assembled contigs with length less than 300 bp were discarded in the following analysis. Genes were predicted over contigs by using MetaGeneMark and redundant genes were removed using CD-HIT with the identity and coverage cutoff 95%, 90%, respectively. To generate the annotation information, the protein sequences of genes were aligned against the functional database using DIAMOND with an E value cutoff of 1×10^{-5} . Differentially enriched KEGG pathways were identified according to reporter scores. An absolute value of reporter scores of 1.65 or higher was used as the detection threshold for significance. The alpha diversity was quantified using the relative abundance profiles at gene, genus and KO levels with R package, respectively. The beta diversity was calculated using Euclidean distance. Statistical analysis of Wilcoxon rank test and Kruskal-Wallis H test were calculated using R project. Raw paired-end reads were deposited into the SRA of the NCBI (accession number: PRJNA983264).

Statistical analysis

The data were expressed as the mean ± standard deviation. All multiple comparison tests (one-way ANOVA or Kruskal-Wallis test) were performed using SPSS 18.0 (SPSS Inc., USA). Statistical significance was considered as $p < 0.05$.